Research Article | Vol. 24, No. 22 | 31 Oct 2016 | OPTICS EXPRESS A1390

Optics EXPRESS

Estimation of daily photosynthetically active radiation (PAR) in presence of low to high aerosol loads: application to OLCI-like satellite data

TRISTAN HARMEL[1,*] AND MALIK CHAMI[1,2]

[1]*Sorbonne Universités, UPMC Univ. Paris 06, INSU-CNRS, Laboratoire d'Océanographie de Villefranche, 181 Chemin du Lazaret, 06230 Villefranche sur Mer, France*
[2]*Institut Universitaire de France, 1, rue Descartes, 75231 Paris Cedex 05, France*
[*]*harmel@obs-vlfr.fr*

Abstract: Estimation of daily photosynthetically active radiation (PAR) is of primary importance for monitoring the ocean primary production and the subsequent production of carbon by phytoplankton at global scale from remote sensing ocean color sensors. On the other hand, aerosol abundance and composition play a critical role in the modulation of PAR. In this study, an original algorithm, so-called OLCIPAR, is proposed for routinely determining the daily PAR from optical satellite sensors such as the OLCI sensor aboard Sentinel-3 (ESA). The OLCIPAR algorithm has been developed to overcome some of the limitations of the current existing methods. In particular, multiple scattering effects induced by the atmospheric layer are taken into account based on exact radiative transfer calculations. Another advantage of OLCIPAR method is to consider a great variety of aerosol models to better account for their optical variability as observed in real world conditions. The OLCIPAR algorithm was applied to the archive of MERIS data, whose sensor is similar to OLCI. The validation of the retrieved daily PAR was carried out based on comparison with the time series acquired by the BOUSSOLE oceanographic buoy moored in the Mediterranean Sea. Results show a regression slope of 1% and an accuracy within 10% which confirms the robustness of the algorithm. The comparison of OLCIPAR retrievals with the products routinely distributed by NASA shows that estimates of PAR differ by up to 20% in the subtropical Atlantic Ocean where important amounts of dust aerosols are present. The improvements brought by OLCIPAR method for deriving the daily PAR could thus permit to better assess the impact of aerosols on reduction of PAR with implications on the estimation of oceanic primary production.

OCIS codes: (010.0010) Atmospheric and oceanic optics; (010.1110) Aerosols.

References and links

1. T. J. Smyth, G. H. Tilstone, and S. B. Groom, "Integration of radiative transfer into satellite models of ocean primary production," J. Geophys. Res. **110**(C10), C10014 (2005).
2. M. E. Carr, M. A. M. Friedrichs, M. Schmeltz, M. Noguchi Aita, D. Antoine, K. R. Arrigo, I. Asanuma, O. Aumont, R. Barber, M. Behrenfeld, R. Bidigare, E. T. Buitenhuis, J. Campbell, A. Ciotti, H. Dierssen, M. Dowell, J. Dunne, W. Esaias, B. Gentili, W. Gregg, S. Groom, N. Hoepffner, J. Ishizaka, T. Kameda, C. Le Quéré, S. Lohrenz, J. Marra, F. Mélin, K. Moore, A. Morel, T. E. Reddy, J. Ryan, M. Scardi, T. Smyth, K. Turpie, G. Tilstone, K. Waters, and Y. Yamanaka, "A comparison of global estimates of marine primary production from ocean color," Deep Sea Res. Part II Top. Stud. Oceanogr. **53**(5-7), 741–770 (2006).
3. V. S. Saba, M. A. M. Friedrichs, D. Antoine, R. A. Armstrong, I. Asanuma, M. J. Behrenfeld, A. M. Ciotti, M. Dowell, N. Hoepffner, K. J. W. Hyde, J. Ishizaka, T. Kameda, J. Marra, F. Mélin, A. Morel, J. O'Reilly, M. Scardi, W. O. Smith, Jr., T. J. Smyth, S. Tang, J. Uitz, K. Waters, and T. K. Westberry, "An evaluation of ocean color model estimates of marine primary productivity in coastal and pelagic regions across the globe," Biogeosciences **8**(2), 489–503 (2011).
4. T. Dickey and P. Falkowski, *Solar Energy and Its Biological-Physical Interactions in the Sea*, J. Wiley (2002), Vol. 12.

#271972 http://dx.doi.org/10.1364/OE.24.0A1390
Journal © 2016 Received 21 Jul 2016; revised 2 Sep 2016; accepted 15 Sep 2016; published 22 Sep 2016

Optics EXPRESS

5. C. D. Mobley and E. S. Boss, "Improved irradiances for use in ocean heating, primary production, and photo-oxidation calculations," Appl. Opt. **51**(27), 6549–6560 (2012).
6. C. R. McClain, "A decade of satellite ocean color observations," Annu. Rev. Mar. Sci. **1**(1), 19–42 (2009).
7. R. T. Pinker, R. Frouin, and Z. Li, "A review of satellite methods to derive surface shortwave irradiance," Remote Sens. Environ. **51**(1), 108–124 (1995).
8. S. Liang, T. Zheng, R. Liu, H. Fang, S.-C. Tsay, and S. Running, "Estimation of incident photosynthetically active radiation from Moderate Resolution Imaging Spectrometer data," J. Geophys. Res. **111**(D15), D15208 (2006).
9. S. Kato, F. G. Rose, S. Sun-Mack, W. F. Miller, Y. Chen, D. A. Rutan, G. L. Stephens, N. G. Loeb, P. Minnis, B. A. Wielicki, D. M. Winker, T. P. Charlock, P. W. Stackhouse, Jr., K.-M. Xu, and W. D. Collins, "Improvements of top-of-atmosphere and surface irradiance computations with CALIPSO-, CloudSat-, and MODIS-derived cloud and aerosol properties," J. Geophys. Res. **116**(D19), D19209 (2011).
10. M. Tripathy, M. Raman, and P. Chauhan, "Estimation of photosynthetically available radiation (PAR) from OCEANSAT-I OCM using a simple atmospheric radiative transfer model," Adv. Space Res. **56**(7), 1441–1452 (2015).
11. C. Guieu, O. Aumont, A. Paytan, L. Bopp, C. S. Law, N. Mahowald, E. P. Achterberg, E. Marañón, B. Salihoglu, A. Crise, T. Wagener, B. Herut, K. Desboeufs, M. Kanakidou, N. Olgun, F. Peters, E. Pulido-Villena, A. Tovar-Sanchez, and C. Völker, "The significance of the episodic nature of atmospheric deposition to Low Nutrient Low Chlorophyll regions," Global Biogeochem. Cycles **28**(11), 1179 (2014).
12. T. Jickells and C. M. Moore, "The importance of atmospheric deposition for ocean productivity," Annu. Rev. Ecol. Evol. Syst. **46**(1), 481–501 (2015).
13. N. Martínez Avellaneda, N. Serra, P. J. Minnett, and D. Stammer, "Response of the eastern subtropical Atlantic SST to Saharan dust: A modeling and observational study," J. Geophys. Res. **115**(C8), C08015 (2010).
14. G. R. Foltz and M. J. McPhaden, "Impact of Saharan dust on tropical North Atlantic SST," J. Clim. **21**(19), 5048–5060 (2008).
15. T. N. Dallafior, D. Folini, R. Knutti, and M. Wild, "Mixed-layer ocean responses to anthropogenic aerosol dimming from 1870 to 2000," J. Geophys. Res. Atmos. **121**(1), 49–66 (2016).
16. The MerMex Group, X. Durrieu de Madron, C. Guieu, R. Sempéré, P. Conan, D. Cossa, F. D'Ortenzio, C. Estournel, F. Gazeau, C. Rabouille, L. Stemmann, S. Bonnet, F. Diaz, P. Koubbi, O. Radakovitch, M. Babin, M. Baklouti, C. Bancon-Montigny, S. Belviso, N. Bensoussan, B. Bonsang, I. Bouloubassi, C. Brunet, J. F. Cadiou, F. Carlotti, M. Chami, S. Charmasson, B. Charrière, J. Dachs, D. Doxaran, J. C. Dutay, F. Elbaz-Poulichet, M. Eléaume, F. Eyrolles, C. Fernandez, S. Fowler, P. Francour, J. C. Gaertner, R. Galzin, S. Gasparini, J. F. Ghiglione, J. L. Gonzalez, C. Goyet, L. Guidi, K. Guizien, L. E. Heimbürger, S. H. M. Jacquet, W. H. Jeffrey, F. Joux, P. Le Hir, K. Leblanc, D. Lefèvre, C. Lejeusne, R. Lemé, M. D. Loÿe-Pilot, M. Mallet, L. Méjanelle, F. Mélin, C. Mellon, B. Mérigot, P. L. Merle, C. Migon, W. L. Miller, L. Mortier, B. Mostajir, L. Mousseau, T. Moutin, J. Para, T. Pérez, A. Petrenko, J. C. Poggiale, L. Prieur, M. Pujo-Pay, P. Pulido-Villena, P. Raimbault, A. P. Rees, C. Ridame, J. F. Rontani, D. Ruiz Pino, M. A. Sicre, V. Taillandier, C. Tamburini, T. Tanaka, I. Taupier-Letage, M. Tedetti, P. Testor, H. Thébault, B. Thouvenin, F. Touratier, J. Tronczynski, C. Ulses, F. Van Wambeke, V. Vantrepotte, S. Vaz, and R. Verney, "Marine ecosystems' responses to climatic and anthropogenic forcings in the Mediterranean," Prog. Oceanogr. **91**(2), 97–166 (2011).
17. M. Mallet, M. Chami, B. Gentili, R. Sempéré, and P. Dubuisson, "Impact of sea-surface dust radiative forcing on the oceanic primary production: a 1D modeling approach applied to the West African coastal waters," Geophys. Res. Lett. **36**(15), L15828 (2009).
18. M. Chami, M. Mallet, and B. Gentili, "Quantitative analysis of the influence of dust sea surface forcing on the primary production of the subtropical Atlantic Ocean using a ten-year time series of satellite observations," J. Geophys. Res. **117**(C7), C07008 (2012).
19. T. Ohde and H. Siegel, "Impacts of Saharan dust on the marine environment in the area off Northwest Africa," in *Remote Sensing of the African Seas* (Springer, 2014), pp. 119–133.
20. T. Ohde and H. Siegel, "Impacts of Saharan dust and clouds on photosynthetically available radiation in the area off Northwest Africa," Tellus B Chem. Phys. Meterol. **64**(0), 17160 (2012).
21. M. Tripathy, M. Raman, P. Chauhan, and Ajai, "Modulation in Ocean Primary Production due to Variability of Photosynthetically Available Radiation under Different Atmospheric Conditions," Int. J. Oceanogr. **2014**, 12 (2014).
22. R. Frouin and R. T. Pinker, "Estimating photosynthetically active radiation (PAR) at the earth's surface from satellite observations," Remote Sens. Environ. **51**(1), 98–107 (1995).
23. R. Frouin, B. A. Franz, and M. Wang, *Algorithm to Estimate PAR from SeaWiFS Data*, Version 1.2 Documentation, Ocean Colour Products (2001).
24. S. Bélanger, M. Babin, and J.-E. Tremblay, "Increasing cloudiness in Arctic damps the increase in phytoplankton primary production due to sea ice receding," Biogeosciences **10**(6), 4087–4101 (2013).
25. B. Chertock, R. Frouin, and C. Gautier, "A technique for global monitoring of net solar irradiance at the ocean surface: 2. Validation," J. Appl. Meteorol. **31**(9), 1067–1083 (1992).
26. R. Frouin and B. Chertock, "A technique for global monitoring of net solar irradiance at the ocean surface: 1. Model," J. Appl. Meteorol. **31**(9), 1056–1066 (1992).

Optics EXPRESS

27. C. Donlon, B. Berruti, A. Buongiorno, M.-H. Ferreira, P. Féménias, J. Frerick, P. Goryl, U. Klein, H. Laur, C. Mavrocordatos, J. Nieke, H. Rebhan, B. Seitz, J. Stroede, and R. Sciarra, "The global monitoring for environment and security (GMES) sentinel-3 mission," Remote Sens. Environ. **120**, 37–57 (2012).
28. R. Frouin and H. Murakami, "Estimating photosynthetically available radiation at the ocean surface from ADEOS-II global imager data," J. Oceanogr. **63**(3), 493–503 (2007).
29. R. Frouin and J. McPherson, "Estimating photosynthetically available radiation at the ocean surface from GOCI data," Ocean Sci. J. **47**(3), 313–321 (2012).
30. E. P. Shettle and R. W. Fenn, "Models for the aerosols of the lower atmosphere and the effect of humidity variations on their optical properties," in *Environmental Research Paper Air Force Geophysics Lab., Hanscom AFB, MA. Optical Physics Div.*, P. Tsipouras and H. B. Garrett, eds. (1979).
31. Z. Ahmad, B. A. Franz, C. R. McClain, E. J. Kwiatkowska, J. Werdell, E. P. Shettle, and B. N. Holben, "New aerosol models for the retrieval of aerosol optical thickness and normalized water-leaving radiances from the SeaWiFS and MODIS sensors over coastal regions and open oceans," Appl. Opt. **49**(29), 5545–5560 (2010).
32. R. C. Levy, L. A. Remer, D. Tanré, S. Mattoo, and Y. J. Kaufman, "Algorithm for remote sensing of tropospheric aerosol over dark targets from MODIS: Collections 005 and 051: Revision 2; Feb 2009," Download from http//modisatmos. gsfc. nasa. gov/_docs/ATBD_MOD04_C005_rev2. pdf (2009).
33. M. Chami, B. Lafrance, B. Fougnie, J. Chowdhary, T. Harmel, and F. Waquet, "OSOAA: a vector radiative transfer model of coupled atmosphere-ocean system for a rough sea surface application to the estimates of the directional variations of the water leaving reflectance to better process multi-angular satellite sensors data over the ocean," Opt. Express **23**(21), 27829–27852 (2015).
34. M. Chami, E. Dilligeard, and R. P. Santer, "Radiative transfer code for the sea-atmosphere system," in *Aerospace Remote Sensing'97* (ISOP, 1997), pp. 476–485.
35. A. A. Lacis, J. Chowdhary, M. I. Mishchenko, and B. Cairns, "Modeling errors in diffuse-sky radiation: Vector vs. scalar treatment," Geophys. Res. Lett. **25**(2), 135–138 (1998).
36. T. Harmel and M. Chami, "Determination of sea surface wind speed using the polarimetric and multidirectional properties of satellite measurements in visible bands," Geophys. Res. Lett. **39**(19), L19611 (2012).
37. A. Morel, "Are the empirical relationships describing the bio-optical properties of case 1 waters consistent and internally compatible?" J. Geophys. Res. **114**(C1), C01016 (2009).
38. J. Pujol, "The solution of nonlinear inverse problems and the Levenberg-Marquardt method," Geophysics **72**(4), W1–W16 (2007).
39. D. Antoine, F. d'Ortenzio, S. B. Hooker, G. Bécu, B. Gentili, D. Tailliez, and A. J. Scott, "Assessment of uncertainty in the ocean reflectance determined by three satellite ocean color sensors (MERIS, SeaWiFS and MODIS-A) at an offshore site in the Mediterranean Sea (BOUSSOLE project)," J. Geophys. Res. **113**(C7), C07013 (2008).
40. R. A. Frey, S. A. Ackerman, Y. Liu, K. I. Strabala, H. Zhang, J. R. Key, and X. Wang, "Cloud detection with MODIS. Part I: Improvements in the MODIS cloud mask for Collection 5," J. Atmos. Ocean. Technol. **25**(7), 1057–1072 (2008).
41. D. Ramon, D. Jolivet, and J. Tan, "Estimating photosynthetically available radiation at the ocean surface for primary production (3P Project): modeling, evaluation, and application to global MERIS," Proc. SPIE **9878**, 98780D (2016).
42. R. Frouin, "A time series of photosynthetically available radiation at the ocean surface from SeaWiFS and MODIS data," Proc. SPIE **8525**, 1–12 (2012).
43. F. M. Bréon, A. Vermeulen, and J. Descloitres, "An evaluation of satellite aerosol products against sunphotometer measurements," Remote Sens. Environ. **115**(12), 3102–3111 (2011).
44. L. A. Remer, D. Tanré, Y. J. Kaufman, C. Ichoku, S. Mattoo, R. Levy, D. A. Chu, B. Holben, O. Dubovik, A. Smirnov, J. V. Martins, R. R. Li, and Z. Ahmad, "Validation of MODIS aerosol retrieval over ocean," Geophys. Res. Lett. **29**(12), 8008 (2002).
45. R. A. Kahn, B. J. Gaitley, J. V. Martonchik, D. J. Diner, K. A. Crean, and B. Holben, "Multiangle Imaging Spectroradiometer (MISR) global aerosol optical depth validation based on 2 years of coincident Aerosol Robotic Network (AERONET) observations," J. Geophys. Res. **110**(D10), D10S04 (2005).
46. G. de Leeuw, T. Holzer-Popp, S. Bevan, W. H. Davies, J. Descloitres, R. G. Grainger, J. Griesfeller, A. Heckel, S. Kinne, L. Klüser, P. Kolmonen, P. Litvinov, D. Martynenko, P. North, B. Ovigneur, N. Pascal, C. Poulsen, D. Ramon, M. Schulz, R. Siddans, L. Sogacheva, D. Tanré, G. E. Thomas, T. H. Virtanen, W. von Hoyningen Huene, M. Vountas, and S. Pinnock, "Evaluation of seven European aerosol optical depth retrieval algorithms for climate analysis," Remote Sens. Environ. **162**, 295–315 (2015).
47. R. C. Levy, S. Mattoo, L. A. Munchak, L. A. Remer, A. M. Sayer, F. Patadia, and N. C. Hsu, "The Collection 6 MODIS aerosol products over land and ocean," Atmos. Meas. Tech. **6**(11), 2989–3034 (2013).
48. C. M. Britton and J. D. Dodd, "Relationships of photosynthetically active radiation and shortwave irradiance," Agric. Meteorol. **17**(1), 1–7 (1976).
49. M. Wild, "Decadal changes in radiative fluxes at land and ocean surfaces and their relevance for global warming," Wiley Interdiscip. Rev. Clim. Chang. **7**(1), 91–107 (2016).
50. A. T. Evan, C. Flamant, M. Gaetani, and F. Guichard, "The past, present and future of African dust," Nature **531**(7595), 493–495 (2016).
51. T. N. Dallafior, D. Folini, R. Knutti, and M. Wild, "Dimming over the oceans: Transient anthropogenic aerosol plumes in the twentieth century," J. Geophys. Res. Atmos. **120**(8), 3465–3484 (2015).

Optics EXPRESS

52. M. Kanakidou, S. Myriokefalitakis, N. Daskalakis, G. Fanourgakis, A. Nenes, A. R. Baker, K. Tsigaridis, and N. Mihalopoulos, "Past, Present and Future Atmospheric Nitrogen Deposition," J. Atmos. Sci. **73**, 2039–2047 (2016).
53. N. Olgun, S. Duggen, P. L. Croot, P. Delmelle, H. Dietze, U. Schacht, N. Oskarsson, C. Siebe, A. Auer, and D. Garbe-Schönberg, "Surface ocean iron fertilization: The role of airborne volcanic ash from subduction zone and hot spot volcanoes and related iron fluxes into the Pacific Ocean," Global Biogeochem. Cycles **25**(4), GB4001 (2011).

1. Introduction

The distribution of phytoplankton biomass is controlled by the availability in nutrients within the water column (e.g., nitrate, phosphate, iron) and by the amount of light entering the ocean. The estimation of the amount of daily radiation available for phytoplankton photosynthesis, so-called daily PAR (Photosynthetically Active Radiation), is of primary importance for estimating the oceanic primary production and the global carbon budget in the open ocean [1–3]. Monitoring of PAR is also important for modeling heat fluxes within the surface oceanic layers [4,5]. Accurate estimation of daily PAR from satellite observations is therefore a prerequisite to provide a global coverage of biogeochemical parameters such as the ocean primary production [6]. Since the incident irradiance at the sea surface is directly related to the atmospheric transparency, which is dependent on the gaseous absorption, cloud cover and aerosol load, an accurate estimation of daily PAR requires a good characterization of the optical properties of the atmosphere [7–10].

In addition to molecular gases in the atmosphere, aerosols generated by multiple continental or oceanic sources participate to modulate the incoming sunlight at the sea surface level. Once deposited, those aerosols can also act as micronutrient supply, thereby, impacting the oceanic plankton systems [11,12]. But, before deposition, aerosols interact with light especially in the visible part of the spectrum resulting in a decrease of the incoming PAR. For example, dust aerosols could affect sea surface temperature (SST) with cooling effects even if dust plumes are often associated with warm air mass [13,14]. Furthermore, anthropogenic aerosols are thought to be capable of significantly affecting SST and the thickness of the mixed layer even under non-cloudy conditions [15]. Despite this recognized impact on ocean waters, the radiative effects of aerosols are still poorly assessed in terms of light availability for marine organisms and potential modification of the intensity of the primary production [16].

Recent studies based on theoretical modeling and SeaWiFS satellite observations showed that desert dust aerosols induce a mean reduction of daily PAR by 15% in the subtropical Atlantic Ocean, with a maximum decrease of daily PAR of 30% off West Africa equatorial coast [17,18]. Note that those results have been recently confirmed by ground-based and in situ measurements [19,20]. Chami *et al.* [18] pointed out that the decrease of PAR due to heavy dust aerosol load could induce a significant decrease of the oceanic primary production between 12% and 17% in the same area. Moreover, a recent sensitivity analysis showed that primary production could be reduced by 38% under realistic heavy maritime aerosol loading depending on the photoadaptation of the primary producers [21]. Nevertheless, all those studies advocated the need of considering realistic aerosol models to provide better estimates of daily PAR and primary production within the full range of possible aerosol loading.

A few algorithms have been developed to estimate the daily PAR from ocean color satellite data [8,22–24]. The pioneer algorithm developed by Frouin and Chertock [25,26] is, to our knowledge, the only one implemented for operational use. The algorithm, which is hereafter referred to as Frouin's algorithm or NASA algorithm, is able to determine the daily PAR for clear sky and cloudy conditions (see section 2). The quasi-single scattering approximation that is used in Frouin's algorithm to calculate the atmospheric reflectance might be questionable in cases of high aerosol loads. It is thus necessary to investigate the potential impact of aerosols on the daily PAR that is retrieved from ocean color sensors.

Optics EXPRESS

The MERIS/ENVISAT (European Space Agency-ESA) satellite mission produced a 10-year archive of global ocean color data from 2002 to 2012. Currently, daily PAR products are distributed by NASA based on Frouin's algorithm. On the other hand, the daily PAR by-product that will be provided by the OLCI/Sentinel 3 sensor (ESA), which has been recently launched in 2016, is not distributed yet. Note that the OLCI sensor has been designed to have similar technical specifications as MERIS sensor, with addition of six extra spectral bands [27]. Some efforts are still needed to propose a robust algorithm to derive the daily PAR from remote sensing data acquired by ocean color satellite sensors like OLCI instrument.

The objective of this study is to propose a robust algorithm, which could overcome some of the limitations of Frouin's algorithm, to estimate the daily PAR over the global ocean from MERIS/OLCI-like satellite sensors for clear sky conditions. One strength of the algorithm proposed in this study, hereafter referred to as OLCIPAR algorithm, is to consider exact radiative transfer calculations of the atmospheric and oceanic radiation to enhance the quality of the daily PAR product under a great range of aerosol models. The paper is organized as follows. First, the Frouin's algorithm is briefly reminded since this method will be used in this study for comparisons. Then, the different steps of the OLCIPAR algorithm are detailed. Validation of OLCIPAR is carried out using both the full MERIS data archive and a time series of in situ measurements of daily PAR. Finally, the influence of aerosols on daily PAR are analyzed in the context of the subtropical Atlantic Ocean.

2. Estimation of daily PAR from MERIS/OLCI-like sensors

2.1 Brief overview of Frouin's algorithm

Frouin's algorithm was initially dedicated to process data acquired by SeaWiFS (NASA) satellite sensor. The method is based on the quasi-single scattering approximation to compute the atmospheric irradiance at ground level. For clear sky conditions, operational processing makes use of a given climatology to obtain the aerosols optical properties in order to calculate the atmospheric transparency in order to ensure operational efficiency and facilitate common data distribution. More specifically, the values of the aerosol optical depth that are used for each pixel of a satellite image are based on a climatology of aerosol relying on a two years averaging (namely, 1997-1998) of SeaWiFS observations. Recently, Frouin's algorithm was applied to other satellite sensors such as GOCI/COMS (KORDI) and Global Imager/ADEOS II (JAXA) [28,29]. However, it has a few limitations regarding the radiative impacts of the aerosols. First, it currently uses the aerosol optical properties of a restricted number of aerosol models, namely nine Shettle and Fenn models (tropospheric, maritime and coastal aerosol models with 3 values of relative humidity for each type of aerosols) [30]. The Shettle and Fenn models might not be sufficiently representative of all types of aerosols [31] that could be found over the globe for providing accurate estimates of the PAR, especially in desert dust turbid areas.

From a mathematical point of view, the top of atmosphere flux ϕ_{TOA} entering the atmosphere-ocean system is expressed as:

$$\Phi_{TOA} = F_0 \cos\theta_s \tag{1}$$

where F_0 stands for the solar extraterrestrial irradiance, and θ_s the solar zenith angle.

Due to the presence in the atmosphere of gaseous absorption, clouds and aerosols, the flux Φ_{surf} that reaches the surface is approximated in Frouin's algorithm using the following expression:

$$\Phi_{surf} = F_0 \cos\theta_s T_a T_g \frac{1-A}{(1-A_s)(1-S_a A)} \tag{2}$$

Optics EXPRESS

where T_a is the transmittance of aerosols and non-absorbing molecules, T_g is the transmittance of gaseous absorption (mainly due to ozone and water vapor), A is the cloud surface albedo, S_a is the spherical albedo of molecules and aerosols, A_s is the sea surface albedo. It is important to mention that the Frouin's algorithm considers that the parameters T_a, S_a and A_s of Eq. (2) are modeled based on the quasi-single scattering approximation (see Eqs. (8) and 9 in [29]). The integration of the flux Φ_{surf} over the visible spectral range (400-700 nm) and over the course of the day provides the daily PAR from Frouin's algorithm.

Knowledge of the aerosol optical depth and aerosol phase function is required to calculate the atmospheric transmittance T_a and the spherical albedo S_a. Knowledge of ozone and water vapor transmittance is necessary to determine the term T_g. The gaseous absorptions are usually taken from ancillary data, typically from ECMWF database or satellite data measured by other sensors. Knowledge of the measured top of atmosphere radiances and atmospheric reflectance are necessary to calculate the term A. Knowledge of the concentration and/or optical properties of the hydrosols, such as the chlorophyll *a* concentration (i.e., phytoplankton biomass), is necessary to calculate the sea surface albedo A_s. The reader is referred to Frouin *et al*. [23] for more details on the Frouin's methodology.

2.2 Consideration of bimodal aerosol models

As highlighted above, a restricted number of aerosol models is used in Frouin's algorithm. However, the influence of the nature of aerosols on the daily PAR can be significant. As an example, the influence of the type and loading of aerosols on the daily PAR is examined with respect to the aerosol optical thickness (AOT) (Fig. 1). Three types of aerosols, namely the sea salt, sulfate-like, and dust-like aerosols, were considered. Their microphysical properties (e.g., refractive indices, effective radius, size distribution) are taken from the Collection 5 (C005) algorithm of the MODIS processing based on the AERONET climatology [32]. The results shown in Fig. 1 were obtained based on radiative transfer calculations using the OSOAA model [33] where polarized state of light is taken into account. The daily PAR (in Einstein m^{-2} day^{-1}) was calculated from the instantaneous PAR ($PAR_{instantaneous}$) as follows:

$$PAR_{\text{instantaneous}}\left(\theta_s\right) = \frac{1}{N_A hc}\int_{\lambda=400nm}^{700} E_d \lambda d\lambda \tag{3}$$

$$PAR_{daily} = \int_{t=0}^{24h} PAR_{\text{instantaneous}}\left(\theta_s\left(t\right)\right)dt \tag{4}$$

where h is the Planck constant, c is the celerity of light, N_A the Avogadro constant, λ is the wavelength ranging from 400 to 700 nm, E_d is the downwelling irradiance just above the sea surface, t is the time over the course of the day, $\theta_s(t)$ is the solar zenith angle at a given time which depends on the latitude, longitude and the date of observation of a given area.

Depending on their nature (e.g., sulfate-like, sea salt, dust-like), the aerosols can induce a relative reduction in the daily PAR reaching over 30% for an AOT value of 1.0 at mid-latitudes. In comparison, the reduction of PAR is around 50% at 70° of latitude. The daily PAR could decrease between 20% (case of sea salt aerosols) and 30% (case of dust-like aerosols) with increasing AOT, which is significant. Therefore, Fig. 1 illustrates the requirement to take into account a great variety of aerosol types (e.g., composition and abundance) to correctly retrieve the daily PAR from satellite data. The OLCIPAR algorithm that is proposed in this study thus considers a significant number of recent aerosol models that are representative of real world conditions. The fine and coarse mode of the aerosols models that were previously designed for aerosol retrieval properties of MODIS satellite sensor (NASA) are used in OLCIPAR algorithm. The microphysical properties of these models such as the refractive indices and the effective radius of the fine and coarse modes (see Table 2a in [32]), are used as inputs of Mie calculations to compute the optical properties of aerosols (e.g., scattering matrix).

Optics EXPRESS

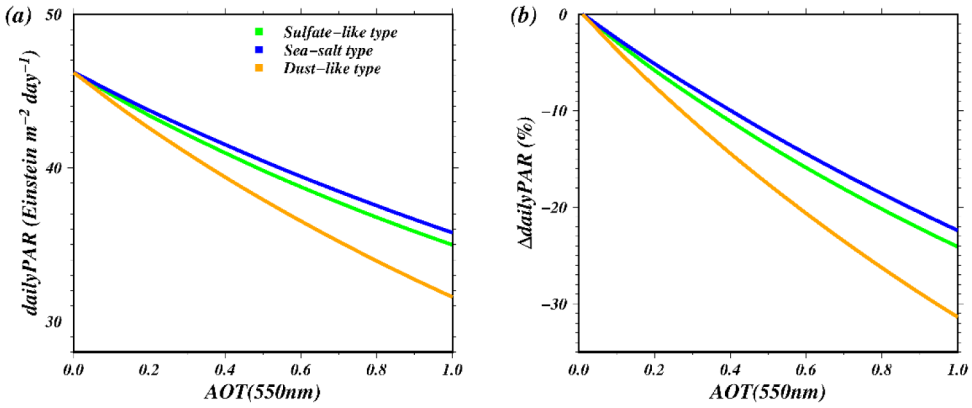

Fig. 1. (a) Influence of the nature of aerosols (e.g., sulfate-like, sea salt, dust-like aerosols corresponding to the models #2, #7, #9 of Levy, Remer, et al. 2009) on the daily PAR (in Einstein $m^{-2}day^{-1}$) as a function of aerosol optical depth (AOT); (b) relative difference between the daily PAR calculated at a given AOT and the daily PAR calculated for an AOT value of 0. The calculations were performed for the latitude 40°N at the vernal equinox.

2.3 Exact radiative transfer computations for radiances, downwelling irradiances and instantaneous PAR

The main principle of the OLCIPAR algorithm is to rely on exact vector radiative transfer calculations for the atmosphere-ocean system with realistic inputs of aerosol optical properties (section 3.1). By doing this way, the contribution of oceanic radiation to the top of atmosphere radiance, namely the radiance induced by hydrosols such as phytoplankton, is taken into account within OLCIPAR at all spectral wavelengths of OLCI and MERIS sensors. The multiple scattering effects occurring in the atmosphere and ocean layers are thus considered by the algorithm (i.e., no single scattering approximation).

The vector radiative transfer model so-called OSOAA model [33] has been used for the computations. The OSOAA model is able to predict the radiance and the polarization state of light for the coupled atmosphere-ocean system for a rough sea surface. Because the polarization induced by molecules or aerosols could have a significant impact on the unpolarized radiance at the top of atmosphere (up to 10%) [34,35], it is of great interest to use a vector radiative transfer model rather than a scalar radiative transfer model to perform accurate calculations of the radiance. Two look up tables (LUT) are generated using OSOAA model to speed up the computation time of the OLCIPAR algorithm and to make it operational for a routine data processing of satellite images. The first LUT (LUT #1) contains the simulated top of atmosphere radiances at each OLCI/MERIS wavelength for a great variety of solar zenith angles, azimuth angles, atmospheric and oceanic conditions. Typically, the solar zenith angle is varied within the range [0°-88°] by step of 2°. The azimuth angle relative to the sun azimuth angle is varied within [0°-180°] by step of 5°. The wind speed value has been set up to 5 m s^{-1}. Note that such a value is consistent with the fact that the majority of the wind speed values encountered over the entire globe in clear sky conditions are within the range 4 to 7 m s^{-1} (see the density plot of Fig. 3(b) in [36]). The aerosol optical depth is varied within the range [0.01-2.0]. Note that the top of atmosphere radiance is calculated for each combination of one fine and one coarse mode of the aerosols defined in Levy *et al.* [32] by varying the fine-mode fraction from zero to 1 continuously, thus providing a great number of realistic aerosol models. The chlorophyll *a* concentration (proxy of the phytoplankton biomass) is varied within the range [0.03-10 mg m^{-3}]. The absorption coefficient of colored dissolved organic matter (a_{CDOM}) at 400 nm is parametrized by a power function of the chlorophyll a concentration [37] and its spectral exponential slope has been fixed to 0.014 nm^{-1}. Because the OLCIPAR algorithm is primarily designed for open ocean

Optics EXPRESS

purposes to better evaluate the amount of carbon produced by phytoplankton over the global ocean, it is thus not our scope to deal with coastal waters in this study, which needs to be addressed specifically due to the optical complexity of these ecosystems. Therefore, mineral-like hydrosols were not included in our simulations.

The second LUT (LUT#2) contains calculations of the ground irradiance and the instantaneous PAR for the same inputs as those used to generate the LUT#1. The ground irradiance is calculated over the visible spectral range [400 nm-700 nm] by step of 10 nm. The instantaneous PAR is obtained by integrating spectrally the ground irradiance over the entire visible range. Note that the instantaneous PAR is defined as the PAR for a given geometry of observation [Eq. (3)] and thus, it is not yet the daily PAR at this stage. The LUT#2 permits to gain operational efficiency since (i) some of the inputs parameters such as the azimuth and viewing angles which are required for calculating the radiance in LUT#1 disappears when calculating the irradiance and (ii) the instantaneous PAR is calculated after the integration of the irradiance over the appropriate spectral range.

2.4 Determination of daily PAR

For every non-cloudy pixels of a satellite image, the aerosol optical depth, the aerosol model (i.e., fine and coarse modes of aerosols, fraction of the fine mode), the chlorophyll *a* concentration and the CDOM (Colored Dissolved Organic Matter) component are determined using a spectral matching technique based on the Levenberg-Marquardt optimization method [38]. The spectral matching technique is applied to minimize the distance between measured data, L_{TOA}^{data}, and simulations, L_{TOA}^{sim}. The distance is defined by the following cost function $\Phi(\mathbf{x})$:

$$\Phi(\mathbf{x}) = \frac{1}{2}\sum_{k=1}^{K}\frac{\left\| L_{TOA}^{data}(\lambda_k) - L_{TOA}^{sim}(\lambda_k, \mathbf{x}) \right\|^2}{\sigma_k} \tag{5}$$

where K is the number of data available per pixel (e.g., spectral radiances), and σ_k an estimator attached to the uncertainty of the data and simulation values defined as follows:

$$\sigma_k = \frac{L_{TOA}^{data}(\lambda_k)}{SNR(\lambda_k)} + \sigma_k^{sim} \tag{6}$$

where SNR is the signal to noise ratio of the given MERIS (or OLCI) band, and σ_k^{sim} the standard deviation of L_{TOA}^{sim} which is calculated by varying the values of the input parameters in the radiative transfer calculations. The minimization of such a cost function [Eq. (5)] permits to retrieve the set of parameters expressed by the state vector $\mathbf{x}$.

The top of atmosphere radiances measured at all spectral bands of MERIS, namely 412, 443, 490, 550, 665, 780, 865 nm, or OLCI (same bands as MERIS and the additional bands of 400, 640 and 1020 nm) are compared with the radiances simulated by the OSOAA model. The proposed algorithm is divided into two distinctive steps in order to facilitate the initialization of the first guess in the non-linear optimization process, as summarized in Fig. 2. One step is dedicated to the retrieval of the aerosol parameters and a second step is dedicated to chlorophyll *a* and CDOM retrievals. In the first step, the measured top-of-atmosphere radiances are compared with simulations to determine the aerosol load and type (couple of fine and coarse modes) based on the minimization of Eq. (5). For this step, the first guess for chlorophyll *a* and CDOM concentrations was fixed to 0.03 mg m^{-3} and 0 m^{-1}, respectively. When the spectral matching is satisfactory, a preliminary set of aerosols parameters is obtained at the end of this stage.

In a second step, the aerosol parameters are then used to determine the values of the chlorophyll *a* and CDOM concentrations. For that purpose, a second comparison is performed

Optics EXPRESS

between satellite measurements and simulations. For that second stage, the ratio between the measured radiance at a given wavelength λ and that measured at the shortest wavelength (412 nm for MERIS, 400 nm for OLCI) is used in Eq. (5), yielding the following cost function to be minimized:

$$\Phi(\mathbf{x}) = \frac{1}{2}\sum_{k=2}^{K} \frac{\left\| L_{TOA}^{data}(\lambda_k)/L_{TOA}^{data}(\lambda_1) - L_{TOA}^{sim}(\lambda_k,\mathbf{x})/L_{TOA}^{sim}(\lambda_1,\mathbf{x}) \right\|^2}{\sigma_k + \sigma_1} \quad (7)$$

Note that the use of such a ratio is relevant since (i) it is better sensitive to phytoplankton and CDOM components and (ii) it is less subject to satellite calibration errors. At the end of the second step, better estimates of oceanic constituents are obtained. They are then introduced again into the first step of the algorithm to adjust the aerosol parameters as an aid to improve the first guess initialization. The iterations between the first and the second steps stop when a minimum value of the sum of the cost functions of the two phases is reached.

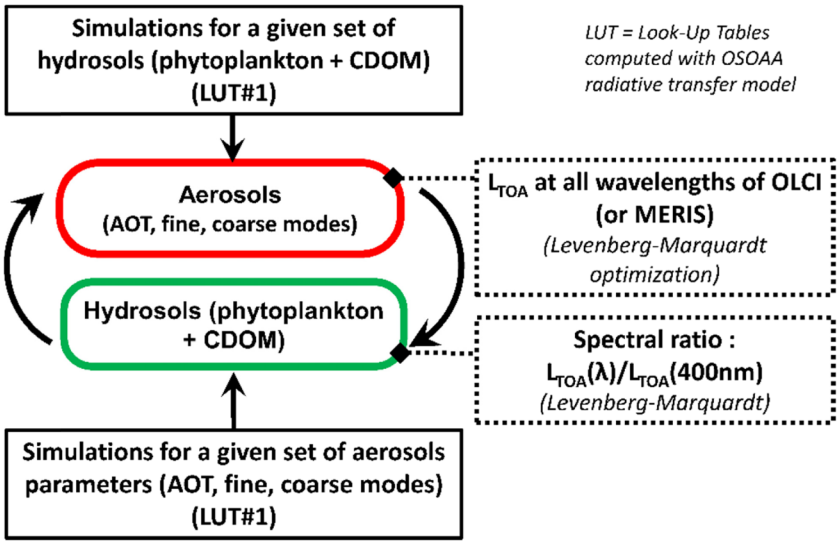

Fig. 2. Flow chart of the part of the OLCIPAR algorithm (use of LUT#1) that is supposed to retrieve the aerosol and oceanic parameters for OLCI- (or MERIS-) like sensors (see text for more details). L_{TOA} is the top of atmosphere radiance, CDOM means Colored Dissolved Organic Matter, AOT means Aerosol Optical Thickness. Note that the algorithm loop stops when the sum of the cost functions of the two phases (determination of aerosol and oceanic parameters) reaches a minimum value.

When the optical properties of aerosols and oceanic constituents are known for a given pixel of the image, the ground irradiance and the instantaneous PAR could be determined from the LUT#2 for the solar zenith angle corresponding to the date and time of the satellite overpass. Since the range of variation of the solar zenith angle over the course of the day could be theoretically calculated for a given satellite pixel, the instantaneous PAR is then integrated over the length of the day using LUT#2 to provide the daily PAR. The time integration is performed using a 15-minute increment over the course of the day [Eq. (4)]. Note that the atmosphere and oceanic optical properties are assumed to be homogeneous over the course of the day. We are aware that this assumption could be questionable especially in areas that are subject to strong daily variability in their cloud/aerosol/hydrosols components. However, there is no exact way to know *a priori* the daily variation of the optical properties from sun synchronous satellite orbit due to their daily revisit period. But, this issue may be circumvented in the future using finer time resolutions of the satellite sensors, such as

Optics EXPRESS

geostationary ones. Figure 3 shows the flow chart of the entire OLCIPAR algorithm (i.e., use of LUT#1 and LUT#2) that is proposed in this study.

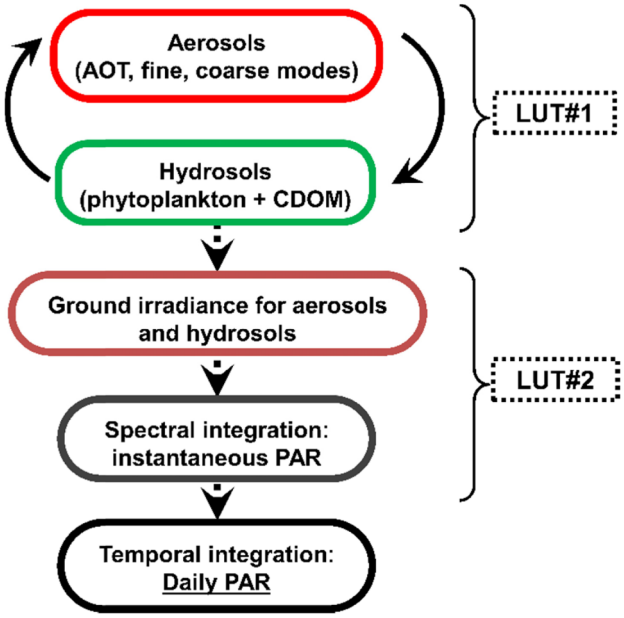

Fig. 3. Flow chart of the entire OLCIPAR algorithm (use of LUT#1 and LUT#2) to estimate the daily PAR (see text for details).

3. Performances of daily PAR algorithms

The validation of the daily PAR is carried out using satellite data acquired by the MERIS instrument (since data from the OLCI sensor are not routinely distributed yet) and comparisons with time series of in situ measurements. For that purpose, the high frequency measurements (typically every 15 minutes) of PAR measured at the BOUSSOLE buoy were used to perform comparisons with the daily PAR retrieved from MERIS data using OLCIPAR algorithm. BOUSSOLE buoy is a permanent mooring which is located at [43°22′N; 7°54′E] in the western Mediterranean Sea at 60 km off the coast (between Nice and Corsica, France) [39]. BOUSSOLE buoy is equipped with many optical sensors, including above-water irradiance and PAR sensors. Note that BOUSSOLE database is publicly available (http://www.obs-vlfr.fr/Boussole/html/home/home.php). Since the instantaneous PAR is measured over the course of the day at BOUSSOLE site, it is thus possible to integrate the PAR data over the time to estimate the daily PAR. BOUSSOLE data were removed from the averaging when the tilt of the buoy is larger than 10°. It is worth noting that the PAR sensor was recalibrated every 6 months by the manufacturer (Satlantic inc.) making the time series consistent over long period acquisitions.

The time series of measurements acquired by the BOUSSOLE buoy started in the early 2000s with routine measurements of PAR since 2003. Over the lifetime of MERIS sensor, satellite and buoy measurements correspond to over 9 years of coincident data (Fig. 4). The amount of data collected is thus sufficiently great to evaluate the consistency and the robustness of the OLCIPAR methodology to derive the daily PAR product. In order to focus the validation exercise on the role of aerosols, the cloudy days were removed from the analysis based on the overcast criteria of BOUSSOLE data [39].

A comparison of OLCIPAR product with the standard NASA product (i.e., Frouin's algorithm) for the same in situ data set has been carried out as well here to quantify the potential improvements of OLCIPAR methodology. Satellite products were averaged over a

Optics EXPRESS

five by five-pixel box (5x5km^2) centered on the BOUSSOLE location. Any pixel masked by the NASA standard processing as "high glint" or by the cloud detection criteria of MODIS processing [40] was filtered out prior to averaging. Figure 4 shows the corresponding time series of daily PAR with colors indicating the aerosol optical thickness retrieved for the OLCIPAR product. First, it is readily visible that the variation of the daily PAR is mainly driven by the solar elevation over the course of the year. The OLCIPAR product is significantly impacted by the aerosol optical thickness relatively to NASA product. This can be easily explained by the fact that the standard NASA processing makes use of an aerosol climatology where the aerosol load is quite low (i.e., for aerosol optical thicknesses typically smaller than 0.3). Second, the OLCIPAR product exhibits a good overall agreement with the in situ data. Note that some of the BOUSSOLE data show dramatically low values for certain days which indicates that all the cloudy condition data were not totally filtered out. Nevertheless, this time series comparison illustrates qualitatively the good representativeness of the OLCIPAR retrievals shedding light on the role of aerosols in clear to moderately turbid atmosphere on modulation of daily PAR.

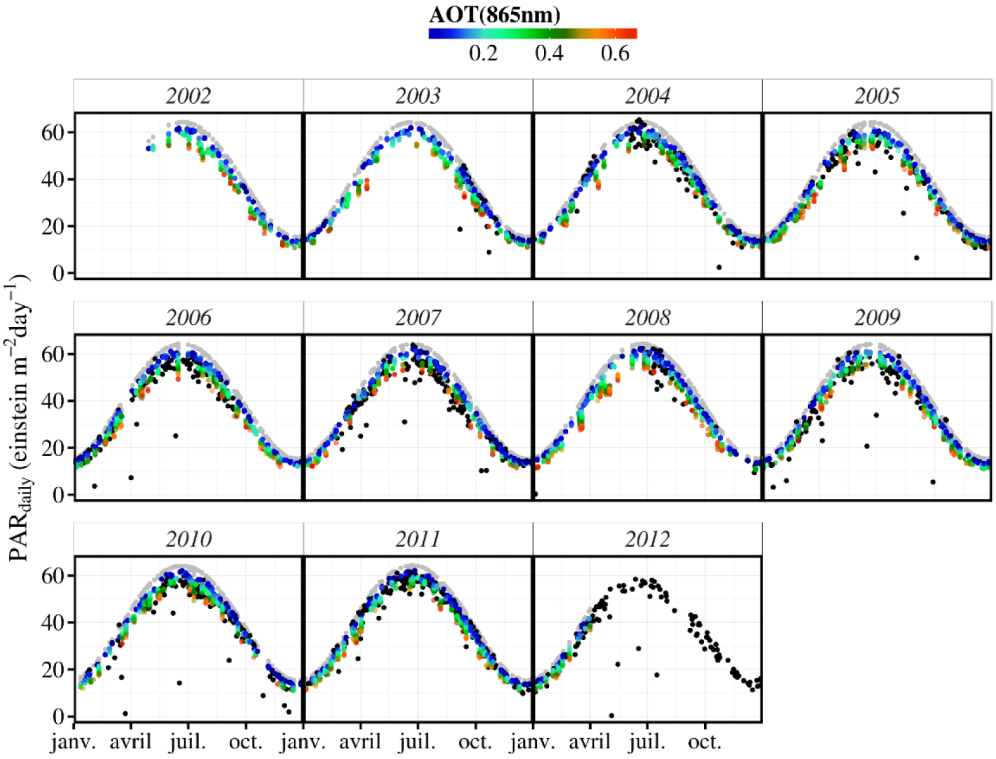

Fig. 4. Daily PAR (in Einstein m^{-2} day^{-1}) time series at BOUSSOLE location for BOUSSOLE data (black), standard NASA MERIS product (grey) and OLCIPAR retrievals (colored dots). Colors refer to the retrieved aerosol optical thickness at 865 nm (see color scale).

Figure 5 shows the matchup comparisons between the daily PAR retrieved from the MERIS and BOUSSOLE time series to express quantitatively the performance of OLCIPAR. The mean of the absolute percentage error (MAPE, in %) and the root-mean-square error (RMSE) are used to evaluate the dispersion of data. The MAPE is defined as follows:

$$MAPE = \frac{100}{N}\sum_{i=1}^{N}\left|\frac{PAR_{daily\_OLCIPAR}(i) - PAR_{daily\_true}(i)}{PAR_{daily\_true}(i)}\right| \quad (8)$$

Optics EXPRESS

Figure 5(a) clearly shows that a significant correlation is observed between OLCIPAR product and in situ measurements (R^2>0.9), thus demonstrating the ability of OLCIPAR to correctly retrieve the daily PAR. The slope of the regression points out an agreement within 1% with a weak bias (less than 1 Einstein m^{-2} day^{-1}). The other statistical parameters (MAPE, RMSE) confirm the weak dispersion of the data; the value of the RMSE is smaller than 5 Einstein m^{-2} day^{-1} and MAPE is around 10%, which is satisfactory. Similar good correlation is observed for the NASA standard distribution (Fig. 5(b)). However, MAPE is less satisfactory with a value of 16% and, more importantly, a large bias is observed with a value of 4.4 Einstein m^{-2} day^{-1} which is about four times the bias observed for the OLCIPAR retrieval. Note that a similar bias was recently observed for daily PAR derived by Frouin's algorithm from MERIS data at the same site [41]. Satisfactory estimates of daily PAR by Frouin's algorithm (Fig. 5) was expected since this latter algorithm has been recently validated for several ocean color satellite missions [29,41,42]. However, the performance of Frouin's algorithm remains slightly lower than that of OLCIPAR. In particular, smaller bias and MAPE is observed for the OLCIPAR data whereas Frouin's algorithm overestimates the daily PAR by 5 to 10%. The use of the quasi-single scattering approximation in Frouin's method to model the downwelling radiation under clear sky might explain the differences with OLCIPAR, which is theoretically more accurate since it accounts for the multiple scattering effects in the atmosphere through exact vector radiative transfer computations.

In order to check the impact of using an aerosol climatology of aerosol optical thickness instead of using instantaneous aerosol retrievals, the Frouin's algorithm was applied considering the aerosol optical properties retrieved from OLCIPAR as inputs (i.e., aerosol optical thickness and Angström exponent). The results are shown in Fig. 5(c). In this latter case, the Frouin's algorithm shows more satisfactory performances than the processing where the aerosol climatology is used (Fig. 5(c)). Figure 5(c) thus reveals that aerosol retrievals obtained from OLCIPAR are meaningful. However, the observed bias is still twice the value of that of OLCIPAR.

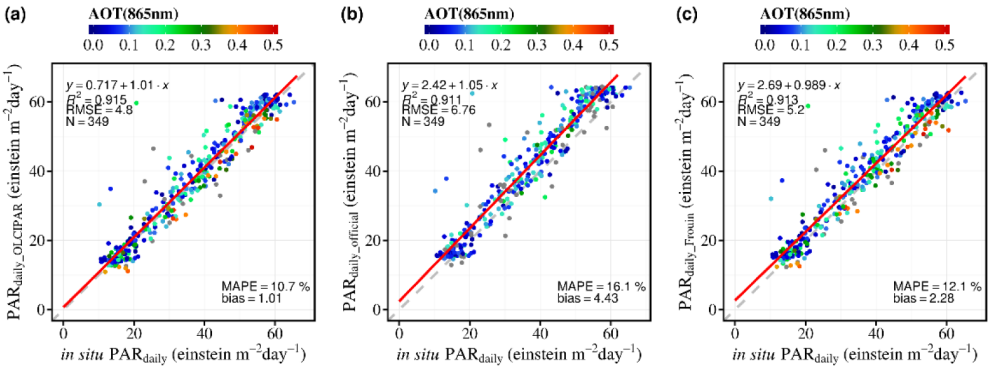

Fig. 5. Quantitative comparison of daily PAR (in Einstein m^{-2} day^{-1}) measured in situ at BOUSSOLE buoy site (western Mediterranean Sea) with the daily PAR derived from time series of MERIS satellite images (from 2003 to 2012) using (a) OLCIPAR algorithm and (b) standard NASA products (i.e., Frouin's algorithm) and (c) Frouin's algorithm applied using the aerosol parameters retrieved from OLCIPAR. N is the number of match up used for the comparison. MAPE and RMSE are the mean absolute percentage error and the root mean square error, respectively. The equation of the regression line (red line) and the coefficient of determination (R^2) are also reported.

4. Influence of aerosols on estimates of daily PAR

The validation exercise demonstrated the importance of considering accurate aerosol retrieval to satisfactorily calculate the daily PAR (section 3). In this section, the role of realistic aerosol

Optics EXPRESS

loads and types on the modulation of PAR is investigated for the subtropical Atlantic Ocean which is an area exposed to both small and large amounts of aerosol.

4.1 Aerosol retrievals

Retrieval of aerosol abundance by OLCIPAR is evaluated against ground-based measurements provided by the AERONET network for the Capo Verde site. For matchup comparison, we followed the *Bréon et al.* [43] recommendations for averaging ground-based and satellite data. All aerosol optical thickness data (AERONET level 2) acquired within the time window of plus or minus 30 minutes the satellite overpass time were used for averaging. The space window considered to extract the ocean pixels corresponds to a square of 50 km side length centered on the AERONET site location. Before averaging, any pixel masked as "high glint" by the NASA processing or "cloudy" based on the MODIS processing criteria is removed. Only averaged values exhibiting low variability in space and time were used for comparison based on the criteria of a relative and absolute standard deviations lower than 20% and 0.1, respectively.

Figure 6 shows the matchup comparison for the aerosol optical thickness at 865 nm retrieved by OLCIPAR applied to the MERIS data with AERONET data. A significant correlation is observed (R^2 >0.81) with a RMSE of about 0.1 and MAPE of 25% which is consistent with other studies [43–46]. Aerosol load is satisfactorily retrieved by OLCIPAR thus leading to confidence for the subsequent derivation of daily PAR. Note that the value of the slope of the regression line suggests a slight underestimation of the highest values of AOT.

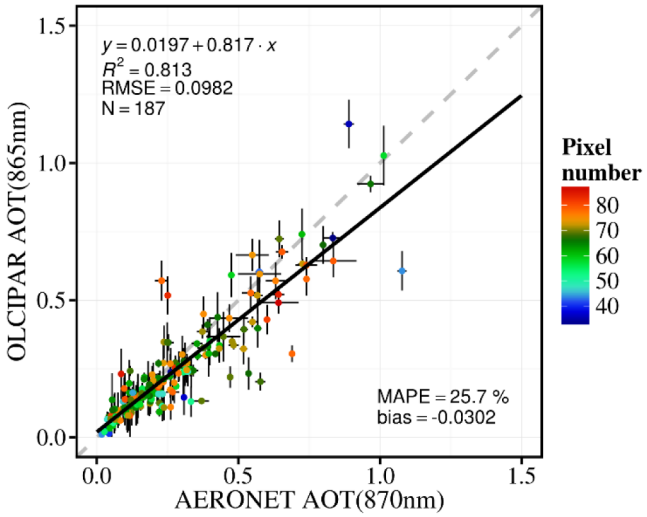

Fig. 6. Matchup between the aerosol optical thickness (AOT) retrieved at 865 nm by OLCIPAR from MERIS data and AOT AERONET level 2 products at 870 nm for the site of Capo Verde (Atlantic Ocean). The number of valid pixels used for the averaging is displayed in color.

To better quantify the discrepancies between OLCIPAR and the standard NASA algorithm, the absolute and relative differences between the daily PAR retrieved by both methods, noted ΔPAR, are examined as a function of the AERONET aerosol optical thickness (AOT) at 550 nm for all the MERIS images acquired over the region offshore the Capo Verde AERONET site (Fig. 7). Interestingly, the variation of ΔPAR with AOT shows a non-linear trend with a significant enhancement of the absolute and relative differences in daily PAR with increasing AOT. Such a relationship is in good agreement with theoretical expectations (see shaded area in Fig. 7). It should be also noted that the low values of the Angström

Optics EXPRESS

exponent retrieved from the AERONET measurements for high aerosol loading suggest the presence of coarse mode aerosols typical of Saharan dust plumes which are likely to occur in this region of the world. Thus, the presence of heavy aerosol loads is not captured by the standard NASA algorithm leading to a daily PAR overestimation reaching more than 20%. Note that a PAR reduction of about 20% was observed as well under Saharan dust plumes from ground-based instrumentation [20].

For clear to moderately turbid atmospheric conditions (AOT < 0.4), the AERONET retrievals show the presence of aerosols with variable Angström exponents which might correspond to several aerosol sources such as biomass burning. For such cases, an accurate consideration of the aerosol load in OLCIPAR leads to daily PAR estimations lower from a few to ten percent than the NASA products. The main differences between OLCIPAR and NASA algorithms are related to (i) the use of aerosol climatology and (ii) modeling of aerosols radiative impacts. Therefore, this study suggests to incorporate into NASA method instantaneous aerosol retrievals instead of averaged values of AOT based on climatology or, at least, a more realistic aerosol climatology accounting for high aerosol load events. Our results also corroborate the need for considering various aerosol models and multiple scattering effects such as OLCIPAR method does. This is an important point since inaccuracies in the retrieval of daily PAR by several percent can have significant implications for the subsequent determination of oceanic primary production at global scale [18,21].

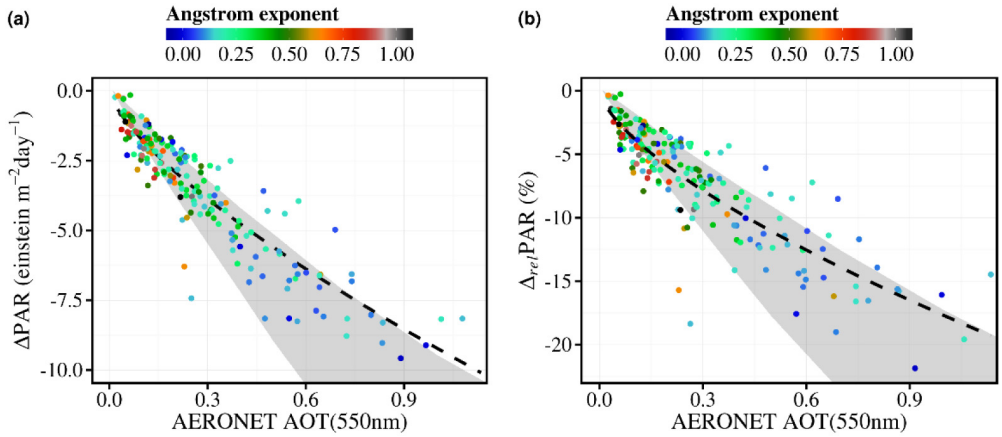

Fig. 7. (a) Absolute and (b) relative differences between standard NASA daily PAR product and OLCIPAR retrievals around the Capo Verde AERONET site with respect to the measured aerosol optical thickness (level 2 AERONET product). Colors indicate the Angstrom exponent of each measurement. Black line corresponds to non-linear fitting of the data. The shaded area corresponds to the theoretical relationship between daily PAR and aerosols (see in Fig. 1).

4.2 Daily PAR reduction over the subtropical Atlantic waters

The OLCIPAR algorithm was applied to the level 1 MERIS archive over the northern part of the subtropical Atlantic Ocean for April 2007. Level 3 binning was then applied to generate the timely averaged values of the aerosol optical thickness and daily PAR. The monthly means of the AOT retrieval is compared to the monthly level 3 MODIS Aqua product generated from the Collection-6 Aqua product [47] (Fig. 8). A qualitative agreement between the two data sets is observed with AOT smaller than 0.2 in the central part of the zone of interest (between 10°N and 30°N) and AOT reaching 0.5-0.6 in the dust aerosol trajectory at the bottom of the image (below ~13°N). In addition to the validation obtained against AERONET data, such a qualitative agreement with the MODIS reference products demonstrates that the OLCIPAR algorithm is reliable for examination of the role of aerosols on the daily PAR modulation at the monthly scale.

Optics EXPRESS

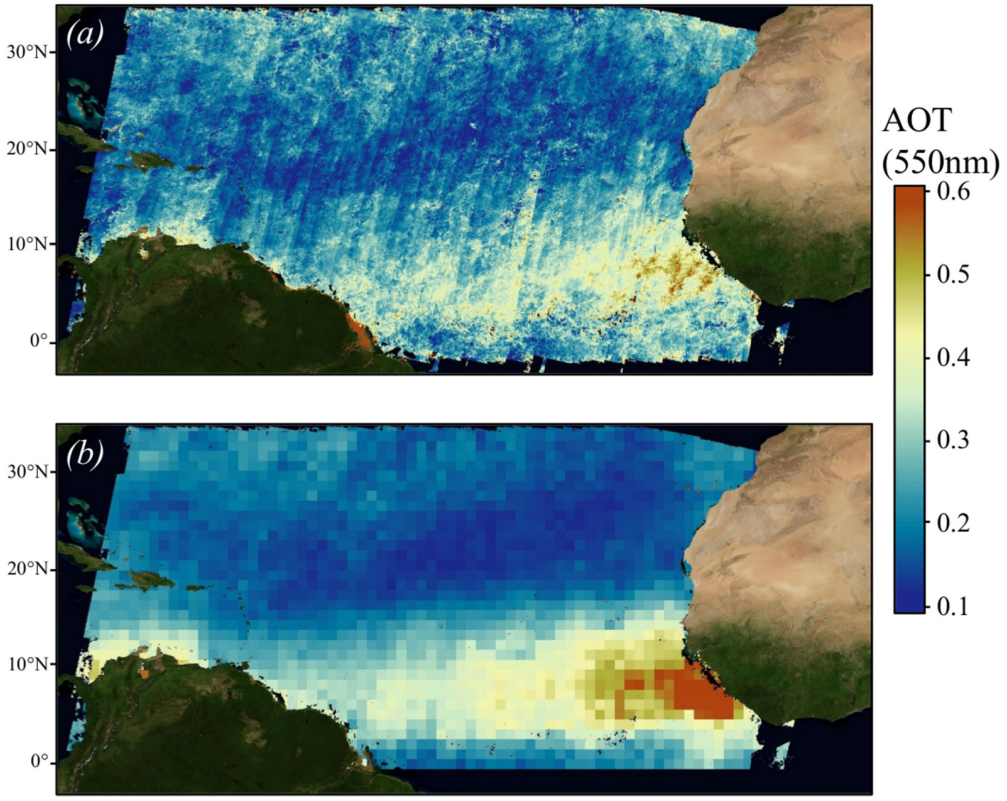

Fig. 8. Monthly mean aerosol optical thickness (AOT) at 550 nm calculated from (a) OLCIPAR retrievals with MERIS and (b) MODIS Aqua standard products (NASA collection 6) for April, 2007 over the subtropical Atlantic Ocean. Spatial resolution is 9-by-9 and 50-by-50 km^2 for MERIS and MODIS products, respectively.

The monthly daily PAR product was derived as well from the NASA OBPG standard distribution after elimination of cloudy or suspicious pixels based on the following seadas masks: HIGLINT, HILT, LAND, CLDICE. Figure 9(a) shows the monthly average of the standard NASA daily PAR for clear sky conditions. Highest values (>56 Einstein m^{-2} day^{-1}) are obtained for the central region where AOT has been seen to be the lowest (<0.2). Conversely, slightly lower values of daily PAR are observed for the region impacted by high aerosol loads (below ~13°N) with values ranging from 53 to 55 Einstein m^{-2} day^{-1}. Note that, at this season, noon Sun elevation is the highest above the equator which means that daily solar irradiance entering at the top of atmosphere is the highest at the equator and decreases with increasing latitude. Thus, if one considers a purely molecular atmosphere, the daily PAR should monotonically decrease from the equator to the poles. An opposite tendency is observed in Fig. 9(a) thus meaning that part of the aerosol influence on PAR is taken into account in the standard NASA daily PAR processing.

Optics EXPRESS

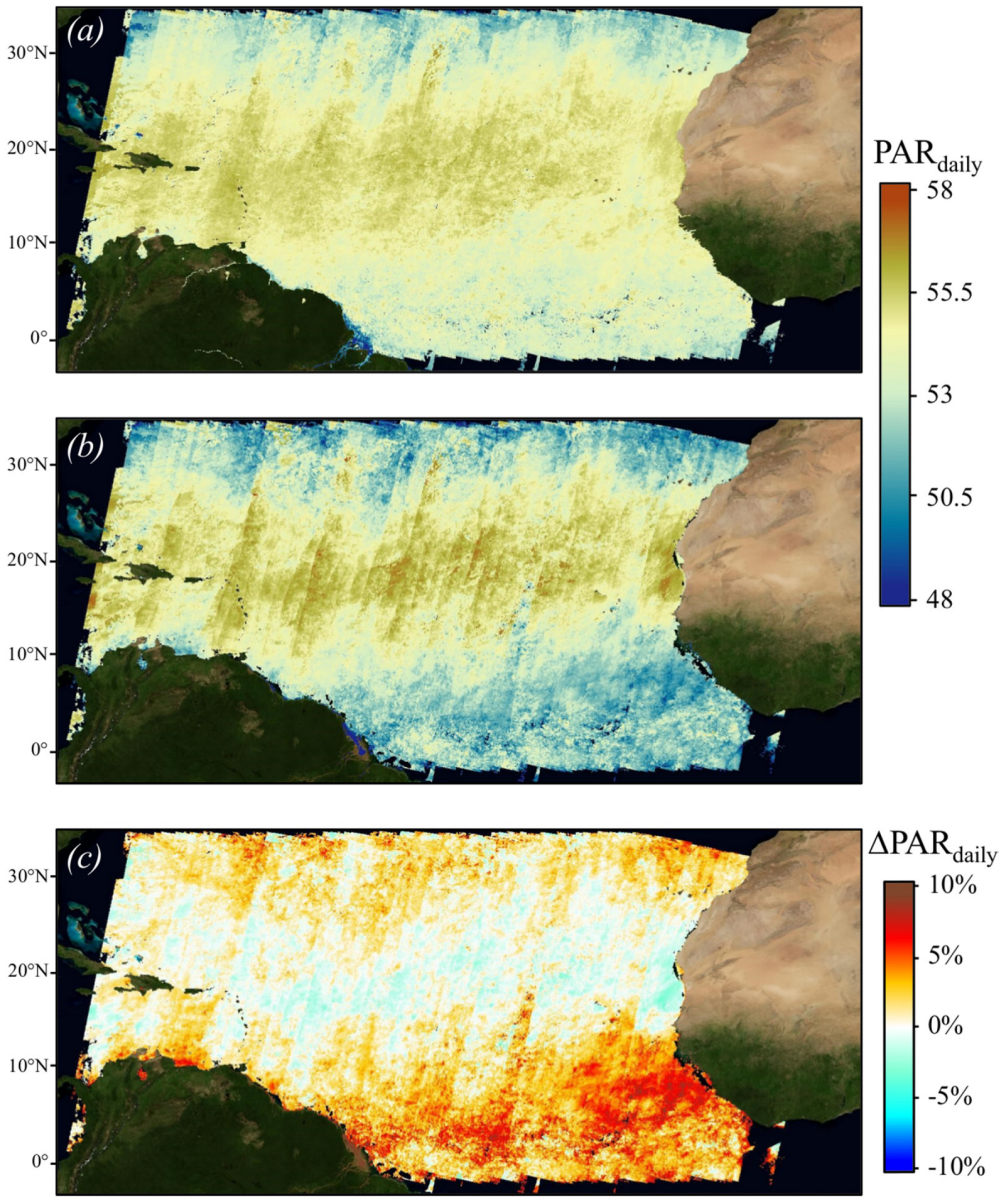

Fig. 9. Monthly mean of Daily PAR (in Einstein m^{-2} day^{-1}) calculated from (a) the standard NASA products and (b) the OLCIPAR retrievals for clear sky pixels of the MERIS images acquired in April, 2007 over the subtropical Atlantic Ocean. (c) Relative difference (in %) between standard NASA product and OLCIPAR monthly mean daily PAR.

The corresponding daily PAR average retrieved by OLCIPAR exhibits much more conspicuous patterns related to the presence of aerosol (Fig. 9(b)). For example, the dust trajectory below 13°N is visible with significantly lower daily PAR values distributed from 48.5 to 52 Einstein m^{-2} day^{-1}. In comparison, the NASA products give values ranging from 53 to 55 Einstein m^{-2} day^{-1} in the same zone. In order to quantitatively compare NASA and OLCIPAR products, the relative differences (in %) were computed as ((NASA) - (OLCIPAR))/(OLCIPAR) *100, as shown in Fig. 9(c). OLCIPAR provides higher PAR values than the NASA product where aerosol load is low (i.e., between 12°N and 25°N).

Optics EXPRESS

Conversely, a tremendous PAR reduction is observed with OLCIPAR for regions with significantly higher AOT (> 0.4) with relative differences reaching 10%.

In parallel, we tried to evaluate the performance of the PAR product derived from OLCIPAR algorithm against the surface shortwave irradiance (SSI) data that is available from the geostationary sensor SEVIRI distributed by EUMETSAT. It should be highlighted that the proportion of photosynthetically active radiation from SSI is variable with intensity of the incident irradiance from 41% to 58% [48], thus resulting to significant uncertainty in the PAR calculation from SSI. The analysis of the ratio of PAR over SSI data taken from the NASA SeaWiFS distribution (both parameters in Einstein m-2 day-1) that we have conducted reveals that there is no trivial conversion of SSI into PAR at global scale. Therefore, a proper conversion of those geophysical parameters obviously deserves a dedicated study which is not the scope of the present manuscript.

Since the representativeness of aerosol impact on PAR within the OLCIPAR processing has been demonstrated earlier in the paper (section 4.1), it could be argued that current NASA products overestimate daily PAR under moderately turbid to turbid atmospheric conditions. This lack of sensitivity in regard to the aerosol content could make difficult the investigation of any significant radiative impacts of aerosols on PAR diminution and on the primary production. On the other hand, solely a very few long-term monitoring radiation sites exist in maritime environments to assess such aerosol impacts on the incoming radiation at sea [49]. As a result, aerosol impacts on PAR will primarily rely on remote sensing capabilities as episodic injections coming from Sahara dust events, biomass burning, or fuel combustion-derived are likely, at the very least, to be modulated in the future years [50–52]. Volcanic dust is another source of high variability in time impacting PAR at the sea surface. However, this kind of aerosol is very poorly considered in aerosol climatology used for deriving the standard NASA PAR product whereas eruptions generate considerable amounts of dusts that have the potential to generate significant short-term strong reduction of PAR and other biogeochemical effects on the oceans [53]. For those reasons and based on the present study, it is highly recommended to consider coincident retrievals of the aerosol load and type instead of aerosol climatology for the estimation of the daily PAR from satellite remote sensing over oceanic areas.

5. Summary and conclusions

An original method, so-called OLCIPAR, has been proposed to estimate the daily photosynthetically active radiation (daily PAR) from remote sensing ocean color sensors for cloud free atmospheres. The objective of this study was to overcome some of the limitations of the current operational algorithm used for deriving the daily PAR from satellite data, the so-called Frouin's or NASA algorithm. For that purpose, the OLCIPAR algorithm uses exact radiative transfer computations through two look up tables to determine the atmospheric optical properties and the subsequent daily PAR. As a result, the multiple scattering effects induced by the atmospheric layer are accounted for in the methodology. Another strength of OLCIPAR is the use of a great number of realistic aerosol models to improve the performance of the retrieval of daily PAR. The use of look up tables within the algorithm is also efficient to ensure a routine operational processing of a large amount of remote sensing data.

The performance and validation of OLCIPAR algorithm was evaluated using comparisons between a time series of MERIS satellite data for which OLCIPAR was applied and in situ measurements acquired by a permanent optical mooring (BOUSSOLE buoy) in the Mediterranean Sea. The discrepancies observed between the satellite derived daily PAR and ground-based measurements is 10%. The results obtained by OLCIPAR algorithm for clear sky conditions were compared with those obtained by NASA algorithm. The results of the comparisons revealed that the daily PAR retrieved by the NASA algorithm, which is based on aerosol climatology, might overestimate the daily PAR by up to 20%. Such overestimation

Optics EXPRESS

may have some significant implications for deriving the oceanic primary production which depends at the first order on daily PAR. In particular, biases in the retrieval of daily PAR may have a significant impact on the phytoplankton photoacclimation, for example, and the subsequent estimates of carbon produced by phytoplankton at global scale. It has been thus argued to rely on coincident retrievals of aerosol optical properties rather than on aerosol climatology to derive the daily PAR.

OLCIPAR algorithm is easily adjustable to any ocean color sensors thanks to the great number of radiative transfer simulations (stored in look up tables), which permits to adapt the algorithm to any spectral configuration. One of the limitations of OLCIPAR algorithm is that it does not apply to cloudy atmosphere. However, the NASA/Frouin's processing could be used for treating the cases of cloudy atmospheres. The portability of OLCIPAR algorithm will enable application to satellite constellations such as that of Sentinel-3 mission or other OLCI-like polar orbiting missions. Thus, combined application of OLCIPAR (for cloud-free atmospheres) and Frouin's algorithm (for cloudy atmospheres) on several satellite acquisitions within a given day would alleviate uncertainties linked to the diel variations of the atmospheric conditions (clouds, aerosol transport). On the other hand, the use of the generated look-up tables and the OLCIPAR algorithm architecture for geostationary satellite data such as SEVIRI (EUMETSAT) or the next GEO-CAPE (NASA) could enable us to contemplate accurate estimation of daily PAR which will account for the diel variations of atmospheric conditions (aerosols, cloudiness…). Such application of OLCIPAR-like algorithms to remotely sensed data showing a high temporal resolution should permit further assessment of the aerosols impacts on PAR reduction at the sea surface and on the estimates of the subsequent primary production.

Funding

Fond Unique Interministériel (FUI) (Marine Collaborative Ground Segment, MCGS)

Acknowledgments

We are grateful to the *Institut Universitaire de France* (IUF) for other financial support. We would like to thank the European Space Agency for providing the MERIS satellite data. We wish to thank Robert Frouin and NASA for making available the Frouin's algorithm used in this study to process the MERIS data. Didier Tanré is acknowledged for his effort in establishing and maintaining the Capo Verde AERONET site. We would like to thank David Antoine (*Laboratoire d'Océanographie de Villefranche*) for making publicly available the data acquired through the BOUSSOLE project (funded by CNES, CNRS-INSU, ESA, NASA, *Université Pierre et Marie Curie*). The authors are grateful to Bernard Gentili and Enzo Vellucci from the *Laboratoire Océanographie Villefranche* (France) for their help in the processing of BOUSSOLE data. We would also like to thank the reviewers for their relevant comments and suggestions.